Pharm Res (2011) 28:1179–1193
DOI 10.1007/s11095-011-0383-z

RESEARCH PAPER

A New Approach to Explore the Impact of Freeze-Thaw Cycling on Protein Structure: Hydrogen/Deuterium Exchange Mass Spectrometry (HX-MS)

Aming Zhang • Wei Qi • Satish K. Singh • Erik J. Fernandez

Received: 19 November 2010 / Accepted: 26 January 2011 / Published online: 8 February 2011

ABSTRACT

Purpose The impact of freeze-thaw (F/T) on structure integrity of protein therapeutics is poorly understood, partially due to lack of methods to detect protein structural perturbations during F/T processing in the frozen state.

Methods A new approach of hydrogen/deuterium exchange was developed to separate and distinguish the specific impact of single freezing and F/T cycling on protein structure, using lactate dehydrogenase (LDH) as model system.

Results In the freezing process, a fraction of LDH molecules that was inversely dependent on protein concentration was observed to partially denature its structure. Local structural perturbations were localized by peptide level HX analysis to the surface residues in segments 91–132, 170–237 and 288–331. In contrast, F/T cycling led to irreversible LDH aggregation with global structural unfolding. Residual solvent-protected structure was only detected in the aggregates for three segments, 13–31, 109–117 and 133–143, that were coincident with the consensus aggregation hotspots predicted by four different algorithms.

Conclusions Results indicate freezing preferentially disturbs local structure at the surface residues, consistent with ice-solution interface-mediated denaturation mechanism. F/T-induced aggregation begins as partial denaturation during freezing, but is accompanied by more comprehensive structural rearrangement during F/T cycling.

KEY WORDS aggregation · freeze-thaw · hydrogen/deuterium exchange · lactate dehydrogenase · structural denaturation

ABBREVIATIONS

DLS	dynamic light scattering
F/T	freeze-thaw
HX	hydrogen/deuterium exchange
HX-MS	hydrogen/deuterium exchange mass spectrometry
LDH	lactate dehydrogenase

INTRODUCTION

Bulk protein storage in the frozen state is commonly utilized in the development and production of protein therapeutics in the biopharmaceutical industry. It increases protein stability by reducing possible degradation kinetics in the frozen state (1). However, formation of bulk ice during freezing can introduce several potential stresses that can damage proteins, primarily in the form of irreversible denaturation and aggregation once the protein has been returned to the solution phase (2–4). These freezing-induced stresses include cold denaturation (5,6), generation of ice-solution interface (7,8) and freezing-induced concen-

A. Zhang • W. Qi • E. J. Fernandez (✉)
Department of Chemical Engineering University of Virginia
102 Engineer's Way
Charlottesville, Virginia 22904, USA
e-mail: erik@virginia.edu

S. K. Singh
BioTherapeutics Pharmaceutical Sciences, Pfizer Inc.
Chesterfield, Missouri 63017, USA

Present Address:
W. Qi
Department of Pharmaceutical Sciences, School of Pharmacy
University of Colorado
Denver, Colorado 80262, USA

tration of protein and solutes which can potentially lead to crystallization (9) and pH shift (10). In the subsequent thawing step, additional damage could be caused by ice recrystallization, which introduces extra interfacial stresses (11). Determination of the primary stress responsible for damage remains a challenging step in rational F/T process development.

To date, the consequences of F/T processing have been well documented, including protein denaturation, biological activity loss, and high molecular weight species formation (2,3,12–14). However, mechanistic analyses of the structural basis for these observations are scarce (7,15), largely due to the lack of effective methods to distinguish protein structural perturbations caused by freezing *vs.* thawing. A frozen protein sample is comprised of two phases: numerous pools of concentrated solute phase (glass) distributed throughout a bulk ice phase. Such a heterogeneous microstructure leads to extensive light scattering and an anisotropic frozen sample (4), precluding analysis by many conventional spectroscopic methods utilized for solution protein analysis. As a consequence, most mechanistic studies of F/T effects on protein structure are carried out on protein samples after going through one or more complete cycles of freezing and thawing, thus providing only indirect evidence of F/T-induced protein damage (2,12).

A few exceptional direct analyses of protein structure in the frozen state, however, have been reported. Gabellieri and coworkers measured dramatic decreases in phosphorescence lifetime at different subfreezing temperatures, suggesting significant conformational changes (4). Later, the same authors found that proteins substantially increased their binding to 1-anilino-8-naphthalene sulfonate (ANS), an extrinsic probe to measure solvent-exposed hydrophobic surface (16,17). More recently, Schwegman *et al.* distinguished protein at the ice-solution interface *vs.* protein remaining in the interstitial solution space by fluorescence microscopy, and demonstrated their alteration in secondary structure by infrared microscopy (7). In a similar study, Dong and coworkers employed confocal Raman microspectroscopy to resolve protein fractions in freezing concentrated solution and at the ice-solution interface, and demonstrated that the latter fraction was structurally altered (18). These studies provided direct support of freezing-induced protein denaturation at the ice-solution interface. However, the above approaches are limited to providing globally averaged structure information, and are unable to identify labile regions or domains in a protein which are most affected by freezing and/or thawing.

Another important concern associated with F/T processing is formation of undesirable high molecular weight species through protein self-association (2,19,20). Protein aggregates in therapeutic protein preparations are increasingly considered a potential cause of adverse effects and/or undesired immune response (21,22). Therefore, protein aggregation must be prevented or minimized throughout expression, purification, and formulation. Since denaturation or destabilization can enhance protein aggregation, the freezing-induced stresses described above can all potentially trigger protein aggregation. Given the accumulated evidence of protein denaturation in the frozen state (7,16,18), it is quite possible that protein molecules that denature during freezing may aggregate in the subsequent thawing step. However, to our knowledge, direct measurements of protein denaturation and aggregation for the same system under F/T processing are not available to test this hypothesis.

In this study, we describe the use of hydrogen deuterium exchange mass spectrometry (HX-MS) to characterize protein structure in the frozen state, specifically to resolve structural effects of freezing-induced protein denaturation from irreversible aggregation after repeated F/T operations. HX-MS has been widely used in solution phase for analysis of protein conformation and dynamics (23–25), as well as structural changes upon a variety of state transitions, such as folding/unfolding (26), ligand binding (27), and self-association (28,29). Further, Li *et al.* carried out hydrogen/deuterium exchange in protein powders to measure the effects of lyophilization and excipients on protein structure (30). However, to our knowledge, HX-MS has not been used for protein conformation analysis in the frozen state. In particular, the use of proteolytic fragmentation during HX-MS analysis enables a higher resolution analysis of protein structure than most conventional spectroscopic techniques (28). In this study, HX-MS was successfully applied to determine solvent accessibility patterns in the frozen state, identifying three labile molecular regions that were most structurally affected during the freezing step. In addition, structural changes in LDH aggregates after repeated F/T operations were also analyzed to identify the potential molecular regions critical for LDH aggregation.

MATERIALS AND METHODS

Materials

LDH (type II, from rabbit muscle, Cat. #: L2500) was purchased from Sigma in the form of crystalline suspension in 3.2 M $(NH_4)_2SO_4$ solution. Deuterium oxide (D_2O) was obtained from Cambridge Isotope Laboratories (99.9% Deuterium, Andover, MA). Tween 80 and 1-anilino-8-naphthalene sulfonate (ANS) were also obtained from Sigma. Thioflavine T (ThT) was from MP Biomedicals (Solon, OH). All other reagents were HPLC purity grade and purchased from Sigma unless otherwise specified.

LDH Sample Preparation

LDH stocks (~11.9 mg/ml in the form of crystalline suspension) were diluted five-fold, and then dialyzed three times against 20 mM citric buffer containing 100 mM NaCl, pH 6.2 to remove $(NH_4)_2SO_4$. The dialyzed LDH solution was centrifuged at 15,000 g for 20 min to remove possible preformed aggregates or crystals. After centrifugation, LDH supernatant was stored at 4°C until use. LDH concentration was determined by measuring A_{280} absorbance using the published extinction coefficient of 1.44 cm^2/mg (31).

High Performance Size Exclusion Chromatography (HPSEC)

HPSEC was performed on a BioLogic DuoFlow chromatography system (BioRad, Hercules, CA). LDH samples (150 μL, sample concentration), either native or aggregated, after a number of F/T cycles were loaded onto a prequilibrated TSKgel SEC column (G3000 SWXL, 7.8 mm×30 cm, Tosoh Bioscience, Bellefonte, PA), and then eluted with 0.3 M NaCl, 50 mM PBS (pH 7.0). The elution flow rate was 1 ml/min. LDH aggregation was expressed as the loss of monomer peak after normalization to the peak area of a native LDH sample. Three replicates were performed for each LDH sample to determine the aggregation level after repeated F/T cycles and the associated standard deviation.

Dynamic Light Scattering (DLS)

LDH aggregate size distribution was measured by dynamic light scattering at 25°C with a DynaPro Plate Reader (Wyatt Technology, Santa Barbara, CA). All LDH samples were diluted to 0.1 mg/ml before measurement. Scattered light intensity was collected at 90° to the incident light. The signal intensity was then averaged over a five-second period to obtain autocorrelation functions using manufacturer's software, DYNAMICS (Wyatt Technology, Santa Barbara, CA). Twenty acquisitions were averaged to make one measurement, and three measurements were conducted for each LDH sample. In data analysis, aggregate size distribution and polydispersity were determined using the regularization method implemented in the DYNAMICS software.

ANS and ThT Binding Fluorescence Analysis

Fluorescence analysis of ANS and ThT binding to F/T-induced aggregated sample was performed at room temperature on a FluoroMax-3 spectrofluorometer (Horiba Jobin Yvon, Edison, NJ). A quartz cell with 5 mm path length (Part number 4ES5X5 Precision Cells Inc., Farmingdale, NY) was used. For ANS binding analysis, 360 μL LDH samples (0.1 mg/ml) were mixed with 40 μL of 100 μM ANS stock solution. Mixed samples were excited at 390 nm, and the emission spectrum was recorded over a wavelength range of 410–600 nm. For ThT binding analysis, 360 μL 0.1 mg/ml LDH samples were mixed with 40 μL of 100 μM ThT stock solution. The excitation wavelength was 446 nm, and the emission spectrum was recorded over a wavelength range of 460–560 nm. All the measurements were performed within 5 min of sample mixing for both ANS and ThT binding, and three scans were performed to obtain an average spectrum for each sample.

HX Procedure to Detect Freezing-Induced LDH Denaturation in the Frozen State

HX labeling in the frozen state was conducted according to the protocol shown in Fig. 1A. LDH stock solution following dialysis and centrifugation was first diluted to desired protein concentrations in H_2O-based citrate buffer (20 mM sodium citrate, 100 mM NaCl, pH 6.2). The diluted LDH sample was then mixed at 1:9 volume ratio with D_2O-based citrate buffer with the same solution composition and pH. The resultant LDH samples had 90% deuterium in solvent and desired final protein concentrations of 0.02, 0.05 and 0.10 mg/ml. To minimize H/D exchange in the solution phase before sample freezing, the final mixing step of LDH solution and deuterium buffer was carried out in the shortest time possible for manual operation (less than 2 s), immediately followed by flash freezing in liquid N_2 for 5 min. Frozen LDH samples were then incubated for the selected labeling time at −10°C. This temperature was chosen because H/D exchange took place within a reasonable experimental time scale (*e.g.* hours to one day). Carrying out the labeling at a temperature lower than the eutectic point of NaCl solution (−21.2°C) would completely freeze the sample (*i.e.* no remaining liquid in the frozen sample), thus leading to an extremely slow H/D exchange rate. Thawing of the deuterium-labeled frozen sample was achieved by adding twice the sample volume of ice-cold 50 mM citrate buffer (pH 2.5) containing 6 M guanidine HCl. Consequently, back exchange was minimized by lowering the pH to ~2.8 during the thawing period. Further, the time for complete thawing of the frozen sample was reduced to 2 min by the high concentration of guanidine HCl.

HX Procedure to Analyze Native LDH and F/T-Induced Aggregates in Solution State

The protocol shown in Fig. 1B was used for labeling of native LDH and F/T induced aggregates. In this protocol, LDH aggregates were prepared by subjecting 0.10 mg/ml LDH samples (200 μL in a microcentrifuge tube) to 10 F/T cycles. Each F/T cycle consisted of 5 min flash freezing in

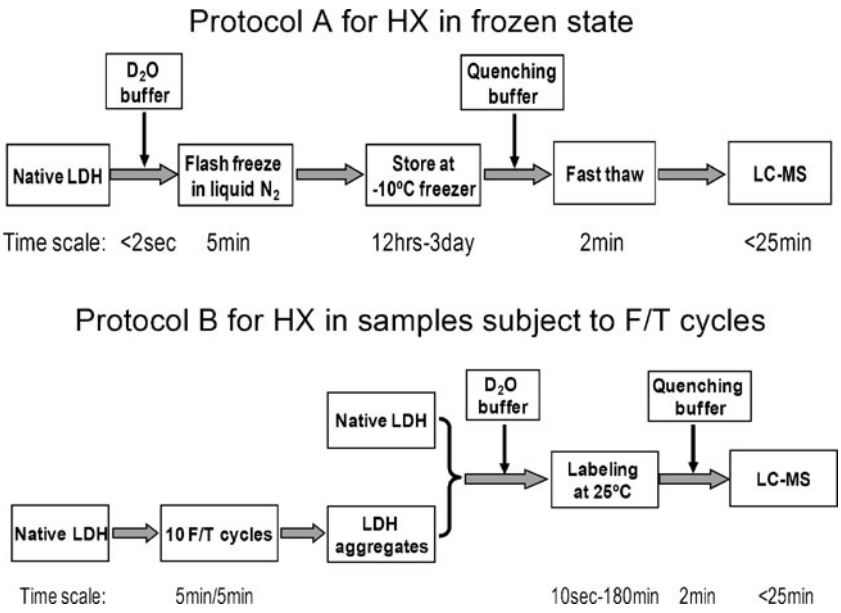

Fig. 1 Two protocols used for HX labeling (Protocol A) in the frozen state, and (Protocol B) after subjection to F/T cycles. The time for each step is designated underneath.

liquid N_2 followed by 5 min thawing in a 25°C water bath. H/D exchange was initiated by mixing native LDH (no F/T cycle) or aggregated (after 10 F/T cycles) samples with D_2O at 1:9 volume ratio to make 90% deuterium in the labeling solution. H/D exchange in solution was maintained at room temperature for different times at 0.17, 1, 10, 60 and 180 min, and then quenched by adding ice-cold quenching buffer (50 mM citrate buffer containing 6 M guanidine HCl, pH 2.5). In this protocol, 6 M guanidine HCl was effective for dissociating LDH aggregates back into monomers for mass spectrometry analysis. High dissolution efficiency was indicated by the comparable MS signal relative to a native LDH sample.

LC-MS for HX Measurements

In both HX protocols in Fig. 1, the same experimental setup was used for mass spectrometry analysis. For whole molecule HX analysis, after quenching of H/D exchange with 50 mM citric buffer (pH 2.5, containing 6 M guanidine HCl), LDH sample was immediately loaded into a sample loop. An isocratic pump delivered the LDH sample in the loop to a peptide trapping column (1 mm ID×8 mm, catalog No. TR1/25108/01; Michrom Bioresources, Auburn, CA) for desalting. After 6 min desalting, a short gradient of acetonitrile (ACN) from 25% to 90% over 7 min (50 μL/min by Surveyor MS Pump, Thermo, San Jose, CA) was used to elute LDH from the trapping column and deliver it to the electrospray ionization ion-trap mass spectrometer (LTQ, Thermo Electron Corporation, San Jose, CA).

In the peptide level HX analysis, an in-line proteolytic digestion was incorporated by including an immobilized pepsin column to the LC setup before the peptide trapping column for desalting. The high concentration of guanidine HCl introduced in the H/D quenching step would be detrimental to the pepsin activity. Therefore, after quenching, five-fold dilution of LDH sample into 0.1% formic acid (pH 2.5) was performed. The peptide mixture resulting from pepsin column digestion was desalted with the peptide trapping column described above, and then separated in a second peptide-resolving column (Kinetex 2.6 μm C_{18}, 2.10× 100 mm, Phenomenex, Torrance, CA). For good peptide separation, a shallower ACN elution gradient (from 15 to 40% over 20 min) was used. All the reporter peptides used for HX analysis were assigned by performing tandem (MS/MS) mass spectrometry, followed by analysis with TurboSEQUEST software. To minimize artifactual isotope exchange during the analysis time, all the columns, loops, and lines were immersed in an ice bath during all the experiments.

The deuteration level for intact molecule and each reporter peptide was calculated by the following equation:

$$D\% = \frac{m - m_0}{(m_{100} - m_0)} \times 100\% \quad (1)$$

where m is the measured centroid mass of the deuterated molecule or peptide after a particular labeling time, and m_0 and m_{100} are the two centroid mass limits of a molecule and reporter peptide from zero-deuteration and full-deuteration control experiments, respectively.

RESULTS

Hydrogen Deuterium Exchange in the Frozen State

The evidence of H/D exchange between LDH and deuterium solvent in the frozen state is shown in Fig. 2. In

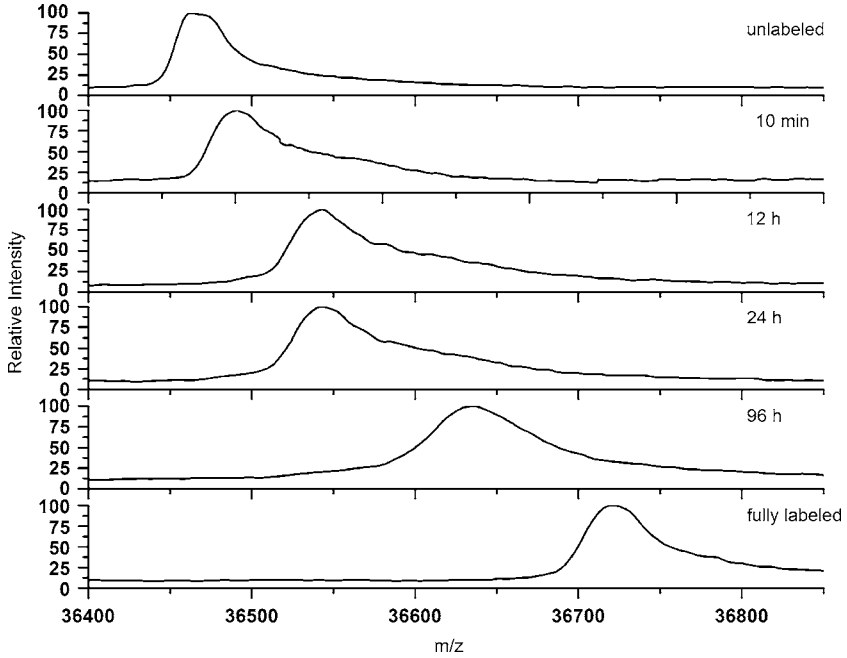

Fig. 2 HX mass spectra of LDH after deuterium labeling at −10°C freezer for a range of time from 10 min to 4 days. Mass spectra at the top and bottom are from control experiments of unlabeled and fully labeled LDH.

this experiment, 0.1 mg/ml LDH was frozen in 90% deuterium buffer using liquid N_2, and then stored in a −10°C freezer for a period of time ranging from 10 min up to 4 days. The degree of deuterium labeling was measured by the mass increase relative to unlabeled LDH by mass spectrometry. As shown in Fig. 2, the molecular mass of LDH increased with incubation time in the −10°C freezer, demonstrating there was continuous incorporation of deuterium into LDH within the experimental time range in the frozen state. The deuteration level calculated by equation (1) increased from 21.8% to 68.3% with the labeling time increasing from 10 min to 4 day. For studies under variable protein and solution conditions, an intermediate incubation time of 12 h at −10°C was selected for LDH conformation analysis in the frozen state for two reasons. First, the observed LDH mass increase from 10 min to 12 h in Fig. 2 suggested that a significant fraction of deuterium labeling was achieved in the frozen sample state during the 12 h incubation, which reduced the effect of H/D exchange in the solution state following LDH sample and D_2O labeling buffer mixing. Second, the deuteration level of LDH after 12 h incubation was not particularly high (38.6%) relative to the fully unfolded control (100%), and it favored the resolution of labeling peaks for native and partially unfolded LDH in the frozen state shown below.

Freezing-Induced LDH Denaturation Analyzed by HX-MS in the Frozen State

Freezing-induced irreversible damages to proteins have previously been shown to be concentration dependent (8,15). In order to find an appropriate LDH concentration where considerable LDH denaturation could be detected by HX-MS, we investigated the effect of freezing on LDH sample concentrations of 0.02, 0.05 and 0.10 mg/ml. In addition, two control experiments with native and fully denatured LDH in the frozen state were performed by freezing 0.01 mg/ml LDH in the presence of 0.01% (w/v) Tween 80 and 6 M guanidine DCl (deuterated by lyophilization), respectively. The freezing procedure, incubation condition and time for two control experiments were identical to these in real LDH sample measurements. The non-ionic surfactant Tween 80 has been shown to fully protect LDH from freezing induced denaturation at such a concentration (8). By contrast, the inclusion of 6 M guanidine DCl provided a control sample of fully unfolded LDH in the frozen state. In Fig. 3, mass spectra obtained for LDH frozen in the presence of Tween 80 (top) and guandine DCl (bottom) represent the lower and upper limits of deuterium labeling for native and fully denatured LDH conformations, respectively.

H/D exchange in frozen LDH samples at three different protein concentrations without Tween 80 or denaturant showed distinct HX behavior as shown in Fig. 3. At 0.1 mg/ml, the mass spectrum of LDH after 12 h labeling exhibited a single major peak with a minor shoulder of heavier molecular mass. The mass increase (*i.e.* deuterium labeling) associated with the major peak was very similar to that of native control with 0.01% (w/v) Tween 80. This indicates that a predominant fraction of LDH molecules essentially maintained native conformation throughout the freezing and incubation period, but meanwhile a small but measurable fraction of LDH explored more solvent-

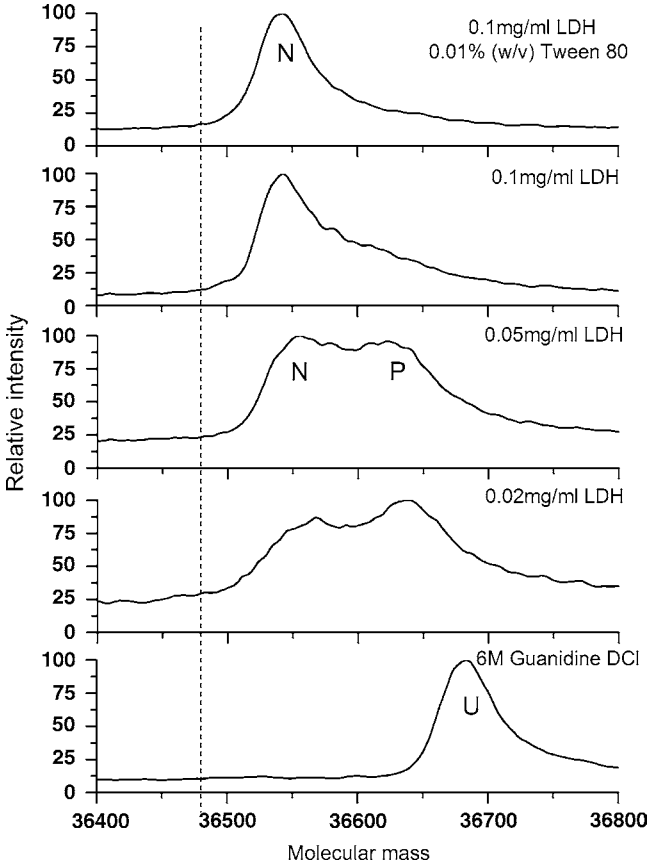

Fig. 3 Deconvoluted mass spectra of LDH after 12 hH/D exchange under −10°C frozen condition. Native (N) and fully unfolded (U) LDH frozen in the presence of 0.01% (w/v) Tween 80 and 6 M guanidine DCl are shown in the top and bottom spectra, respectively. Native and partially denatured LDH from three frozen samples are labeled as N and P under corresponding mass peak in the middle panel. The vertical dashed line indicates LDH molecular mass without deuterium labeling.

accessible conformations. At lower LDH concentration, the high mass shoulder grew and became a peak of comparable area at 0.05 mg/ml, and exceeded the area of the low mass peak at 0.02 mg/ml. The second, heavier mass peak exhibited a degree of deuterium labeling around 79.9±4.8%. This value was far higher than the value for the low mass peak of native-like LDH in the frozen state (42.1±3.9%), but still substantially lower than 100% deuterium labeling of the fully unfolded LDH. This result suggested that a fraction of LDH molecules partially unfolded its native structure during the freezing process, leading to increased solvent accessibility in at least one-third of its sequence.

Local Structural Perturbations Elucidated by Peptide Level HX-MS

The HX analysis of intact LDH shown in Fig. 3 identified a partially denatured LDH species in the frozen state, but does not indicate the site where local native structure was lost in the freezing process. To obtain this information, peptide level HX analysis was carried out in parallel for frozen LDH samples by implementing an online proteolytic fragmentation step as described before (28). In this study, 34 reporter peptides, covering about 94% of LDH sequence, were identified and examined in HX to elucidate local structural perturbations caused by the freezing process.

Similar to the whole molecule analysis, each column in Fig. 4 compares deuterium labeling of the same reporter peptide obtained from four LDH preparations: native control (containing Tween 80), two samples at 0.10 and 0.05 mg/ml concentration, and a fully unfolded control (labeled in the presence of 6 M guanidine HCl). Based on the labeling behavior for two LDH samples relative to native and fully denatured controls, the 34 reporter peptides were categorized into four groups. A representative from each group is shown in each of the four columns of Fig. 4. The first group had very similar deuterium labeling as to that of the native control, suggesting that local native structure in this segment was not disturbed by the freezing process. Reporter peptide 133–142 (shown in the left column of Fig. 4) is a representative of this group. In the second group, reporter peptides showed an intermediate degree of deuterium labeling between the native and fully unfolded controls, indicating partial loss of native structure within this region. In contrast for the third group, the native control and two samples had deuterium labeling very similar to that of the fully unfolded control, suggesting that those reporter peptides were fully solvent-accessible in the native conformation. Consequently, HX analysis cannot assess if freezing causes local structure perturbation to these regions. Finally, reporter peptide 288–301 from the last group (the right column in Fig. 4) exhibited two labeling peaks in mass spectra as observed in whole molecule analysis (Fig. 3). Further, the high mass peak is close to the fully unfolded control, and the low mass peak close to native control in terms of deuterium labeling. This observation suggested the presence of two local molecular conformations with native and unfolded structure in this region. In combination with whole molecular HX analysis above, it can be deduced that the partially denatured LDH species in the frozen state must have freezing unfolded structure in the regions identified by the fourth group of reporter peptides. In other words, reporter peptides from the fourth group are the labile regions susceptible to freezing stress.

Fig. 5A shows the locations of the four groups of reporter peptides in the LDH sequence. The first to fourth groups are represented by blue, slate, red and yellow bars, respectively. Thus, Fig. 5A shows the pattern of local structure perturbations to LDH by the freezing stress. In this pattern, there is a fraction of partially denatured LDH molecules in which three labile regions 107–132, 170–204

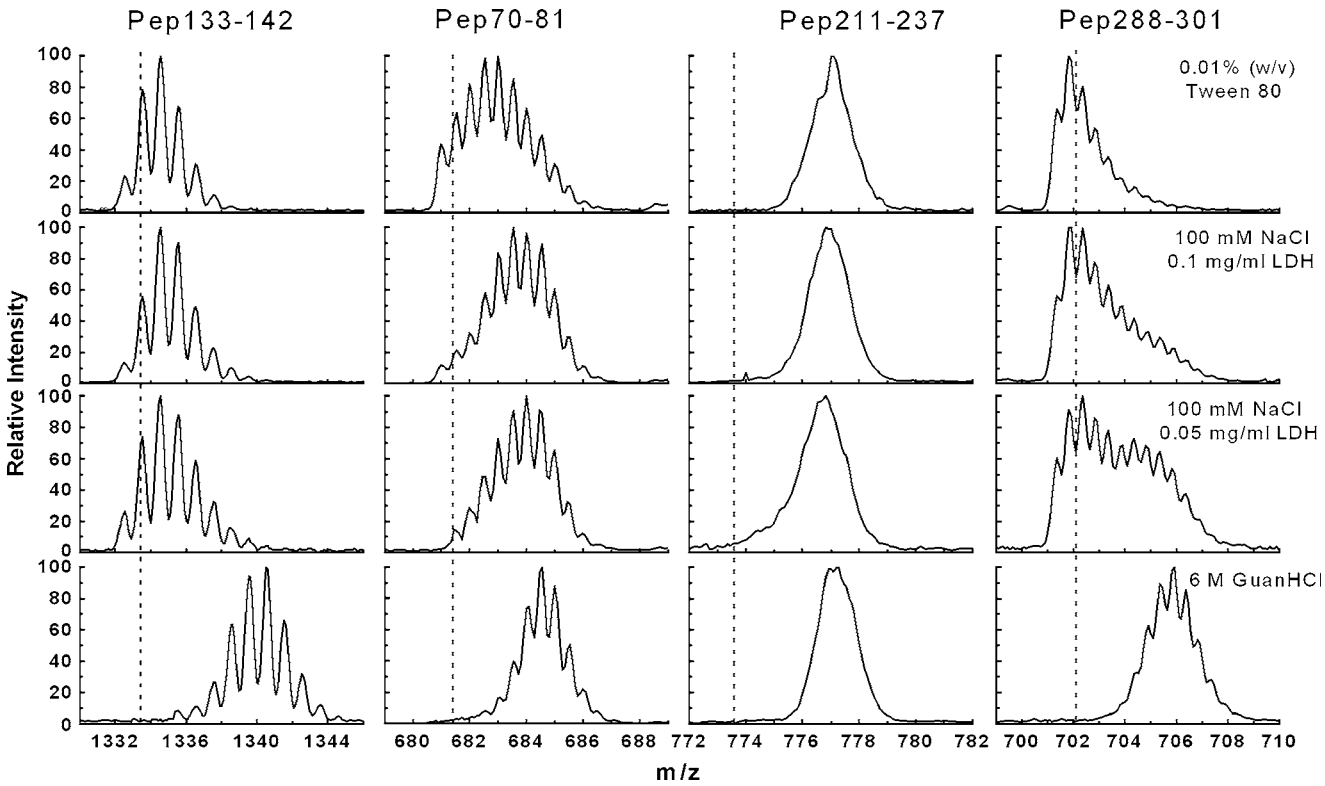

Fig. 4 Representative mass spectra of four groups of reporter peptides with distinct HX labeling behavior. Each column shows mass spectra of one representative reporter peptide from native, two-sample, and fully unfolded LDH in the frozen state. The vertical dash lines represent unlabeled mass for each peptide. Representative reporter peptide for each class is labeled above the columns.

and 288–331 (in *yellow bars*) were subjected to almost complete native structure loss by the freezing stress. Two of them are adjacent to the fully solvent-accessible regions 91–106 and 205–237 (in red bars) in native LDH structure, and the third is located at the C-terminus. This observation indicates that in LDH, the residues adjacent to the most solvent-exposed sequence are more susceptible to freezing denaturation. It is noteworthy that there are several overlapping peptides throughout the sequence which have similar behavior, serving to increase confidence in the observed solvent accessibility pattern.

In Fig. 5B, the same HX pattern is mapped on one chain of LDH tetramer structure (PDB: 3H3F). It shows the yellow freezing labile regions and red solvent-accessible regions are spatially clustered together on the solvent exposed surface of native crystal structure. By contrast, the blue and slate regions which were less affected by freezing stress are located in the structural core or at the interface in contact with other monomers within the tetramer.

LDH Aggregation Induced by Repeated F/T Operations

LDH aggregation induced by repeated F/T operations was analyzed by HPSEC and DLS. The effects of two parameters on LDH aggregation were investigated: the number of F/T cycles and protein concentration in the solution. Fig. 6A shows the HPSEC elution profiles of 0.1 mg/ml LDH samples after being subject to 1, 5 and 10 F/T cycles. The elution peak of LDH tetramer was normalized to that of native LDH sample (without F/T cycle). As expected, the residual native LDH decreased with the number of F/T cycles. After 10 F/T cycles, there was only a small fraction of native LDH (4.2± 2.3%) remaining in the solution. In the elution profile, a minor peak between 11–12 min was observed for the native LDH sample. It may be attributed to a small fraction of dissociated LDH tetramer in solution. For the aggregate samples, a second peak corresponding to LDH aggregates was not observed throughout the elution process, probably because the formed aggregates were too large to enter the SEC column. This was supported by the fact that treatment of LDH aggregate sample with 6 M guanidine HCl almost completely recovered LDH molecules in the HPSEC analysis, and centrifugation operation could precipitate the LDH aggregates from solution as suggested by Fig. 6B. Notably, in these HPSEC analysis, 4 M guanidine HCl solution was used as the mobile phase. LDH tetramer in this mobile phase was presumably dissociated into monomeric state, there-

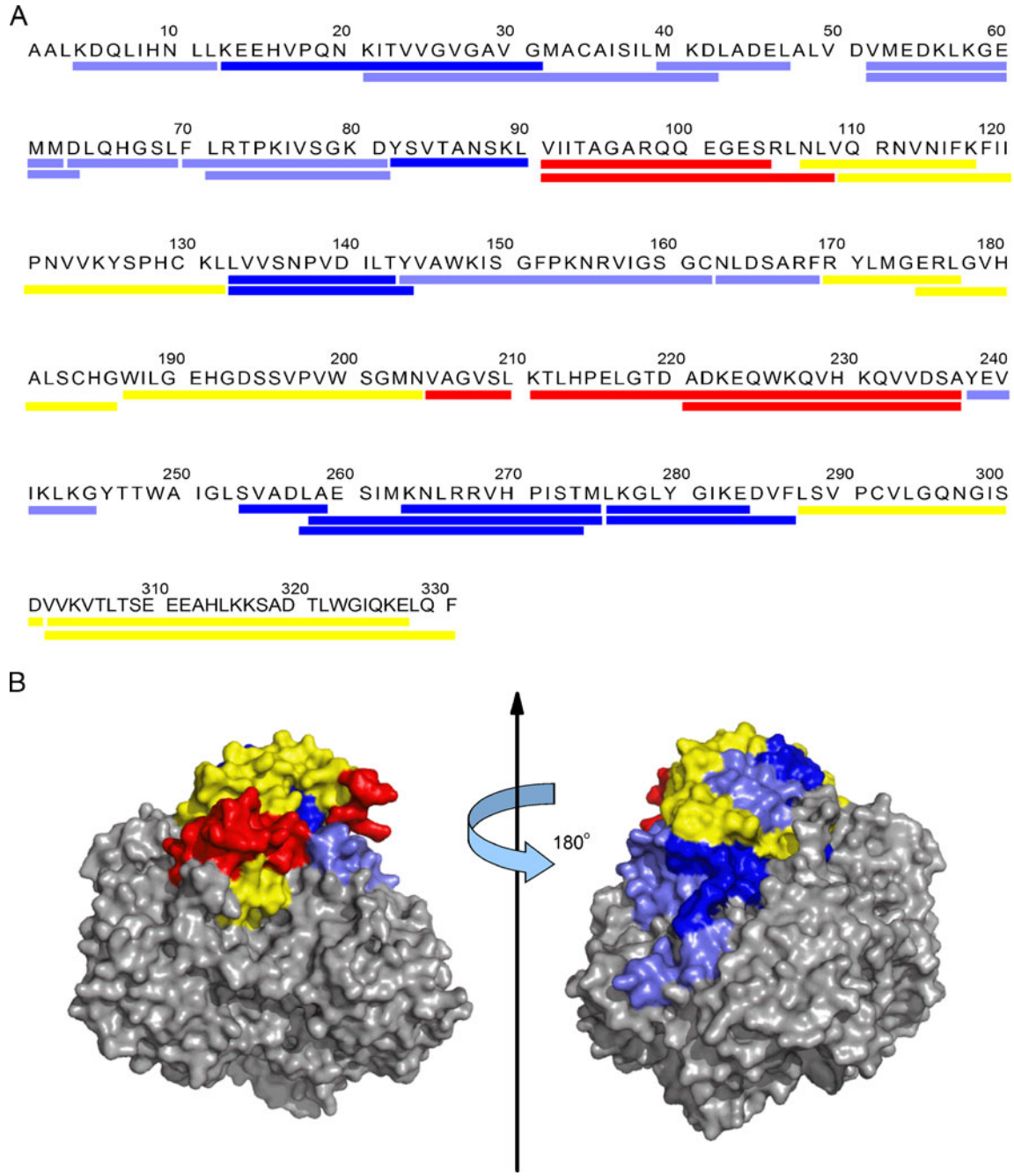

Fig. 5 Local structural perturbations to LDH molecule by the freezing process as mapped by HX pattern on primary (**A**) and 3D crystal (**B**) structure. Color code from blue, slate, red to yellow represent reporter peptides and molecule regions with native-like conformation, subject to partial denaturation, fully solvent accessible and with most substantially structure denaturation, respectively. In panel B, only one molecule chain in the native tetramer structure (PDB: 3H3F) is color-coded for better view.

fore showing a longer retention time (~12 min) which was similar to the minor peak observed in normal HPSEC analysis in Fig. 6A. The large size of F/T induced LDH aggregates was also suggested by DLS measurement in Fig. 6C, which showed average hydrodynamic radius of from ~300 to ~2,500 nm increasing with F/T cycles.

The effect of protein concentration on F/T-induced aggregation is shown in Fig. 6D. The percentage of remaining native LDH in F/T-treated samples (10 cycles), measured from the native peak area, increased from 4.2 ± 2.3% to 92.3 ± 3.5% when the LDH concentration increased from 0.1 mg/ml to 1.0 mg/ml in the initial solution. This inverse dependence of F/T-induced aggre-

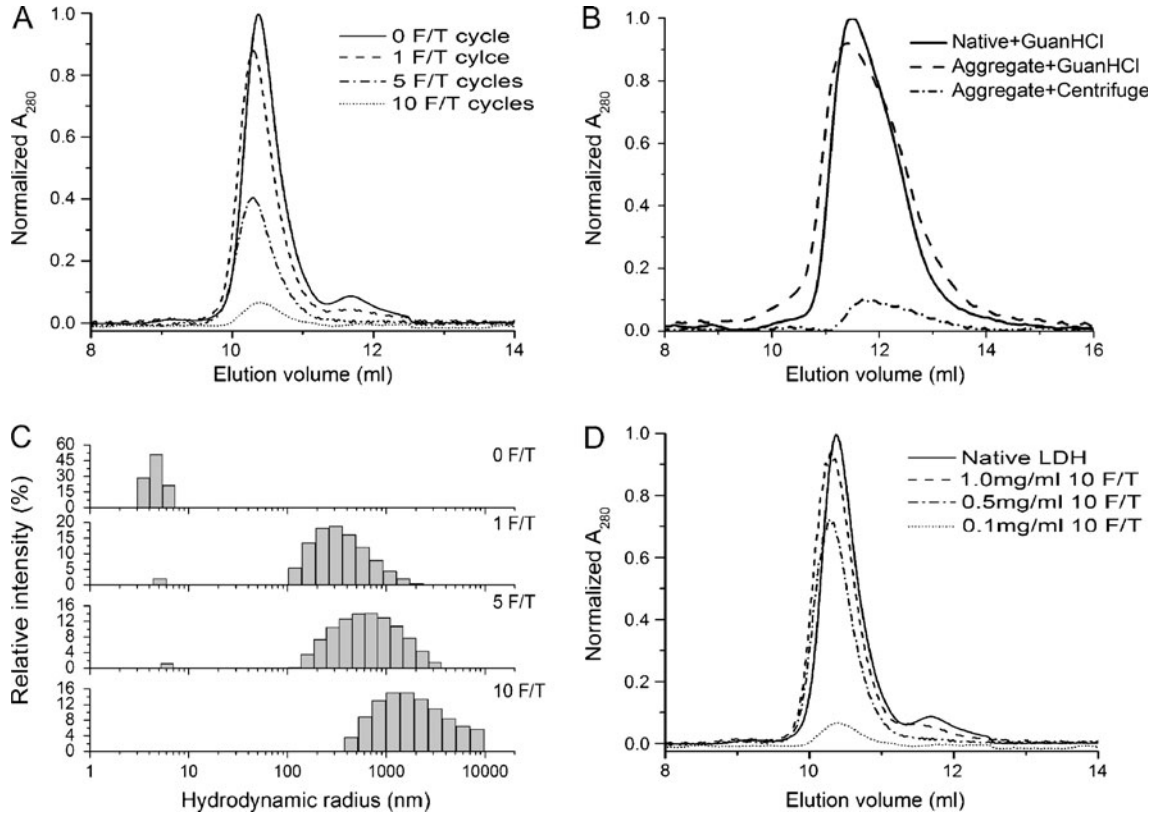

Fig. 6 HPSEC and DLS analysis of F/T induced LDH aggregation. **A**: the effect of F/T cycle number on LDH aggregation; **B**: treatment of 6 M guanidine HCl or centrifugation to LDH aggregate samples on the HPSEC elution profile; **C**: hydrodynamic radii of F/T-induced LDH aggregates after 1, 5 and 10 cycles measured by DLS; **D**: the effect of LDH concentration on F/T-induced aggregation. All the HPSEC elution profiles were normalized to corresponding native LDH sample without subjected to F/T cycle.

gation on protein concentration has been observed previously (32).

LDH Aggregate Structure Characterized by Dye Binding

Structure of F/T-induced LDH aggregates was also analyzed by binding of two extrinsic fluorescent dyes: ANS and ThT. ANS measures protein solvent-exposed hydrophobic surface area (33), while ThT tends to bind rather specifically to amyloid-like structures (34). According to the HPSEC analysis in Fig. 6A, 0.1 mg/ml LDH solution after 10 F/T cycles was almost completely aggregated, and thus can be used as "pure" aggregate sample for structure analysis. Fig. 7A demonstrates that ANS exhibits a substantial increase in signal intensity and slight blue shift in the maximum emission in the presence of LDH aggregates produced by repeated F/T cycles relative to native LDH or protein-free buffer controls. These two spectral changes indicate increased ANS binding, suggesting that LDH molecules exposed more hydrophobic residues in the aggregated form than in the native state. In the ThT binding assay (Fig. 7B), increased fluorescence intensity was observed for LDH aggregates relative to native counterpart in the whole wavelength range; however, a typical prominent fluorescence peak with maximum emission at approximate 482 nm was not observed (35). This suggests that F/T-induced LDH aggregates do not possess amyloid-like structure.

LDH Aggregate Structure Characterized by Intact HX-MS

The structure of F/T-induced LDH aggregates was further characterized by intact molecule HX-MS. Fig. 8 shows the HX mass spectra of native LDH and aggregated sample with 10 F/T cycles after labeling times of 0.167, 10, and 180 min. The dotted spectra on the top and bottom panels are those from unlabeled and fully labeled LDH. From Fig. 8, it can be seen that both native and aggregated LDH increased in molecular mass with deuterium labeling time. Further, the aggregated samples (dot-dashed spectra) exhibited a far higher degree of labeling than native LDH at all the labeling times. After 180 min, the aggregated LDH had a degree of deuterium labeling around 90.0± 5.2% relative to 57.6±3.2% for the native LDH. The

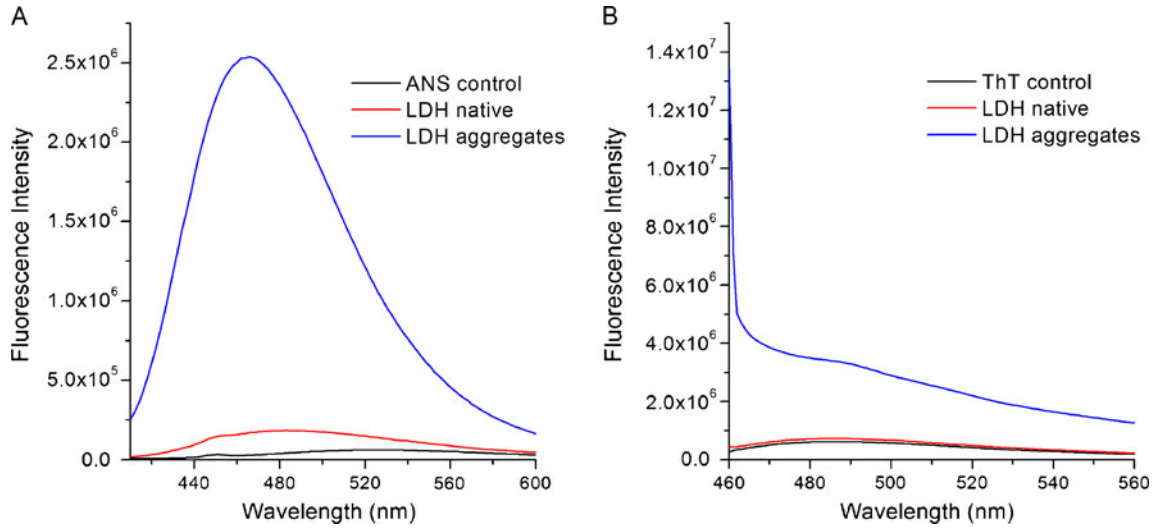

Fig. 7 Fluorescence spectra of ANS (**A**) and ThT (**B**) binding to native LDH and F/T-induced aggregated sample (prepared by 10 freeze-thaw cycles of 0.1 mg/ml LDH solution), respectively.

dramatically increased deuterium labeling is consistent with ANS binding fluorescence analysis in Fig. 7A, both suggesting a more solvent-exposed molecular conformation in the aggregated state. Further, in the mass spectra of LDH aggregates, there is a minor low mass shoulder that shows native-like deuterium labeling. The fraction of this low mass shoulder was comparable to that of residual native LDH in the HPSEC analysis (Fig. 6), suggesting this shoulder represents LDH retaining native structure after 10F/T cycles.

Local Structure of LDH Aggregates Characterized by Peptide Level HX-MS

Peptide level HX-MS was carried out to analyze LDH aggregate structure in more detail. Fig. 9 compares the time course HX pattern measured for native LDH and F/T-induced aggregates at the peptide level. In the color-coded HX pattern, each horizontal block under the LDH sequence presents HX of one reporter peptide. Five color bars represent labeling at times of 0.167, 1, 10, 60 and

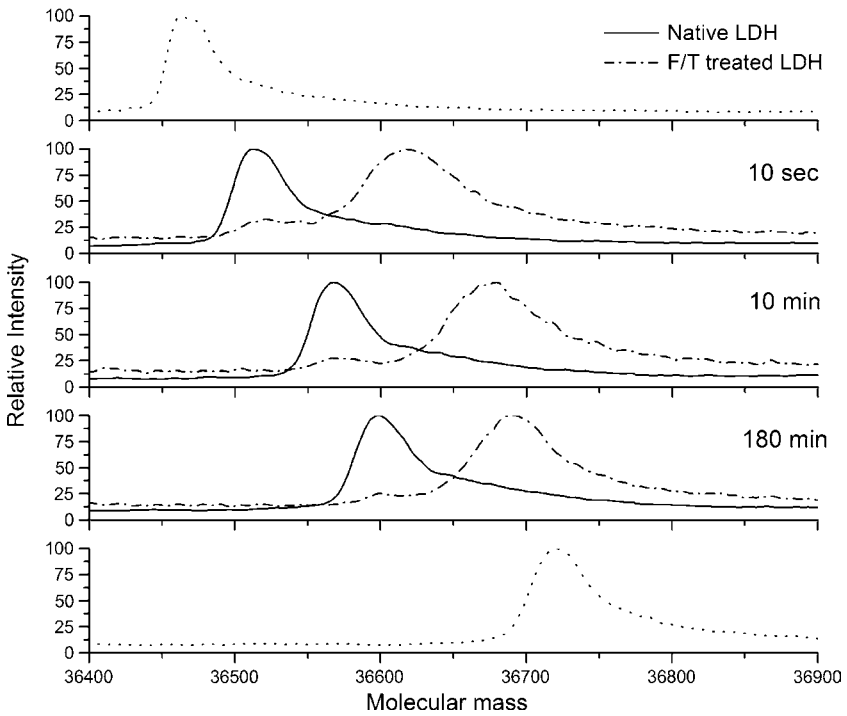

Fig. 8 HX mass spectra of native LDH and F/T-induced aggregated sample obtained after 10 s, 10 min and 180 min deuterium labeling. The dotted spectra in the top and bottom panels are unlabeled and fully labeled controls, respectively.

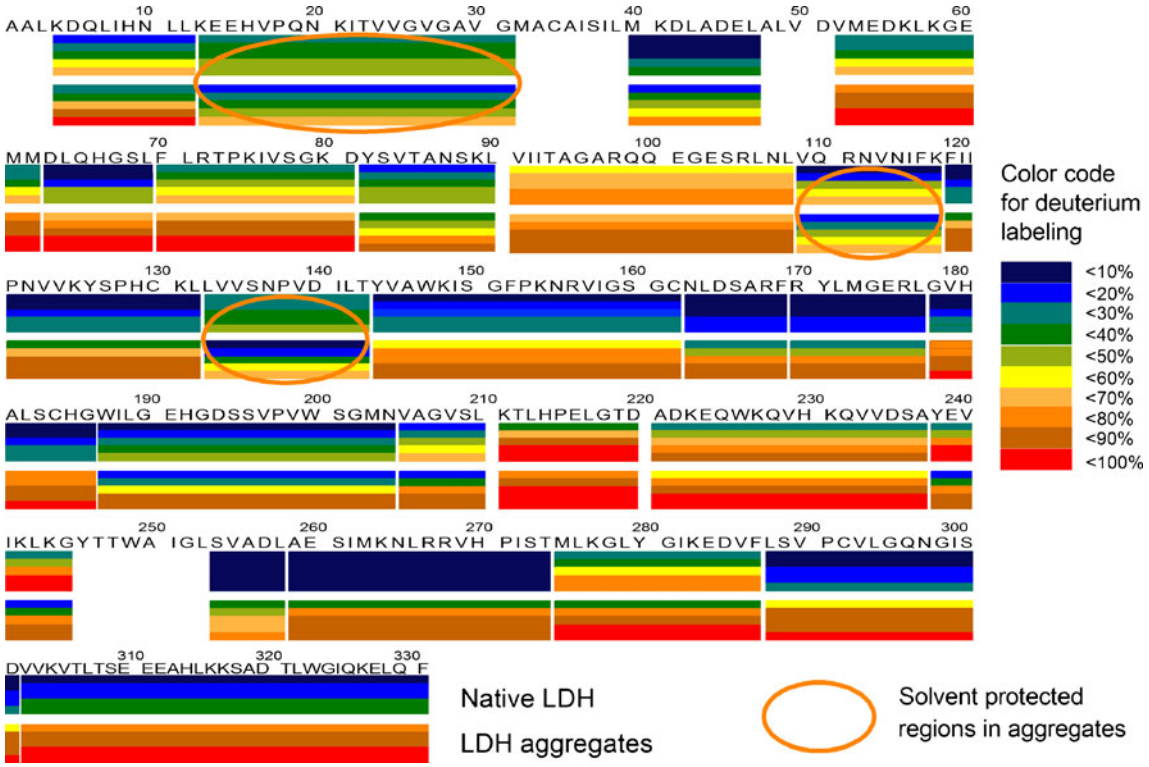

Fig. 9 Peptide level HX pattern of native LDH (*top block*) and F/T-induced aggregates (*bottom block*) measured in solution. Each horizontal block represents one analyzed reporter peptide; each block contains five color bars representing the degree of labeling at five different labeling times (from top to bottom, 10 s, 1 min, 10 min, 60 min and 180 min). The deuterium labeling of each reporter peptide at each labeling time point is color-coded using the scale as shown in the right insert. Reporter peptides with deuterium labeling less than 70% after 180 min for LDH aggregates are circled as solvent-protected regions in the aggregates.

180 min (from top to bottom), respectively. For each reporter peptide two blocks are shown, comparing of the HX pattern between (top) native LDH and (bottom) F/T-induced aggregates. The color code for the degree of deuterium labeling is shown on the right side of the figure.

For native LDH, it is seen that reporter peptides from different molecular regions vary substantially in measured deuterium labeling, ranging from less than 10% up to almost 100% as determined by eq. 1 in the Materials and Methods. The highly variable HX pattern indicates that native LDH has a molecular conformation with a wide range of solvent accessibilities. By contrast, reporter peptides of F/T-induced LDH aggregates showed a more uniform HX pattern featured by consistently high deuterium labeling, more than 80% in most of the sequence after 180 min of labeling. The high solvent accessibility across LDH sequence observed for the aggregates was consistent with the substantially increased global deuterium labeling seen at whole-molecule HX analysis in Fig. 8, both suggesting a more solvent accessible conformation of LDH in the aggregated form.

However, in F/T-induced aggregates, the three reporter peptides 13–31, 109–117 and 133–143 stood out as showing significantly retarded H/D exchange relative to the rest of LDH sequence. In particular, none of the above three peptides was among the reporters with the most solvent protection in the native state (163–177, 254–274 and 288–301). The retarded HX measured for the three reporter peptides in the aggregates could be attributed to three possible sources: local residual native structure, specific cross-β interactions in amyloid-like aggregates, and other kinds of intermolecular contacts in protein aggregates. The fact that the new set of most protected peptides in LDH aggregate was completely different from the most protected regions of the native state suggests that reporter peptides 13–31, 109–117 and 133–143 were not protected by residual native structure. Further, the ThT binding assay in Fig. 7 suggests that amyloid-like contacts are not present in LDH aggregates. In addition, the highly rigid structure of cross-β interactions in amyloid aggregates usually leads to a far lower degree of deuterium labeling than these measured for the three protected peptides (28,36–38). Thus, it would appear most likely that reporter peptides 13–31, 109–117 and 133–143 formed new intermolecular contacts in F/T-induced LDH aggregates, leading to the retarded HX relative to other solvent exposed regions.

Correlation of Solvent-Protected Regions and Predicted Aggregation Hotspots

While our results cannot definitively distinguish between the above three explanations for solvent protection in reporter peptides 13–31, 109–117 and 133–143, intermolecular interactions between largely unfolded monomers or oligomers are a distinct possibility. Recently, prediction of polypeptide segments with high propensity to self association for given protein sequence has been made based on synthetic polypeptide aggregation data. Four of these 'aggregation predictors' are TANGO (39), PASTA (40), AGGRESCAN (41), and PAGE (42). Consensus regions predicted by these predictive tools in combination may indicate the polypeptide segments in protein sequence that are most likely to introduce intermolecular interactions responsible for protein aggregation (43). The four calculators above were applied to the LDH sequence (all using default parameters by program developers) to test if the three solvent-protected regions were predicted as consensus aggregation hotspots. Fig. 10 shows the consensus regions predicted by at least three out of the four predictors. All three solvent-protected regions are predicted at least partially to overlap consensus aggregation hotspots, though there are three other consensus hotspots predicted, which might be considered "false positives."

DISCUSSION

Freeze-thaw processing can cause irreversible damage to labile proteins, such as loss of biological function, denaturation, and/or high molecular weight aggregate formation (2,3,7). However, the structural basis of these different forms of irreversible damages to proteins is poorly understood, particularly the effects of the freezing step, due to the lack of an effective technique to characterize protein structure in the frozen state.

In this study, we have shown that hydrogen/deuterium isotope exchange (HX) can be applied to protein structure analysis in the frozen state at both the whole molecule and peptide levels. This new application of HX-MS was demonstrated for a model protein LDH that has been extensively used for freeze-thaw studies (7,15). As shown in Fig. 3, the structural denaturation of LDH by freezing was indicated by the formation of a new LDH species with more solvent exposure than native LDH, but distinctly less than fully unfolded LDH frozen with 6 M guanidine HCl. This partially denatured LDH species increased in proportion with reducing protein concentration, agreeing well with concentration dependence of protein damage found during F/T processing previously (11,32). The inverse concentration dependence of LDH denaturation was also consistent with the denaturation mechanism mediated by an ice-solution interface during freezing. In such a

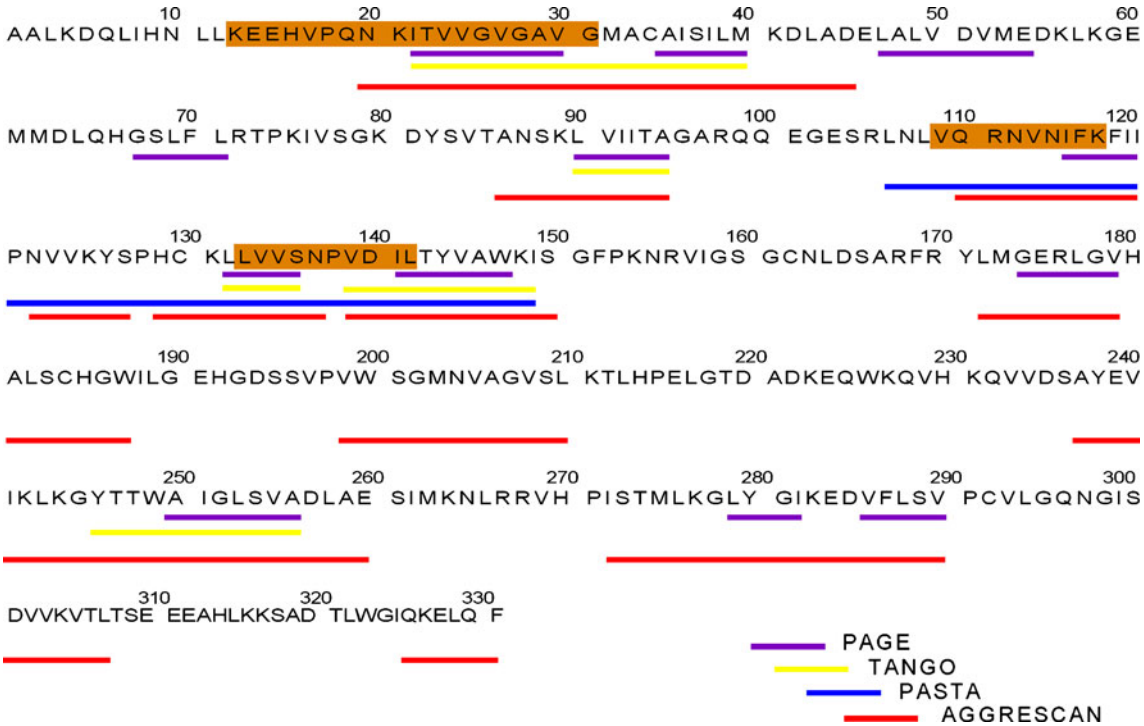

Fig. 10 LDH aggregation hotspot prediction by four different computational algorithms. Bars of each color under the sequence show the aggregation-prone regions predicted by one corresponding computational algorithm. Consensus regions predicted by at least three of four computational algorithms were identified as aggregation hotspots. Three solvent-protected regions in LDH aggregates identified by peptide level HX are highlighted on the sequence.

mechanism, the ice surface could be saturated by protein adsorption, resulting in a relatively lower fraction of denatured protein at high protein concentrations.

In the frozen state, population distributions of specific conformations (*e.g.* folded and partially unfolded) have not been reported before. In most previous studies, the impact of freezing on protein structure was determined based on the alteration of protein secondary and/or tertiary structure in the frozen state detected mainly by FT-IR and fluorescence (4,16,17). These techniques, however, provide only a signal averaged over all the protein molecules in the frozen state. Thus, determining population distributions and identifying partially denatured states has not been straightforward. In a recent study, confocal Raman microscopy was used to spatially resolve different protein conformations at the ice-solution interface *vs* in the freeze-concentrated liquid (18). However, it was not feasible to determine the quantitative distribution of these two protein conformations in the frozen state. Conversely, the HX-MS approach shown in Fig. 3 provided at least semi-quantitative distribution information of two LDH populations as affected by protein concentration in the frozen state. Furthermore, this technique makes it possible to analyze the effects of a variety of freezing parameters, such as supercooling, freezing rate and excipient addition, on the distribution of two LDH populations in the frozen state (data not shown).

Another important advantage of the HX-MS approach is the ability to explore structural changes at the peptide level, thus making it possible to identify molecular regions that are labile to freezing stress. As shown in Fig. 5, the local structural perturbations to LDH by freezing were revealed. In this pattern, the blue and slate regions from partially denatured LDH had very similar deuterium labeling to the native LDH, suggesting they retained local native-like conformations in the frozen state. Two red regions, 91–108 and 205–237, had nearly full solvent accessibility in both native and partially denatured LDH, making it impossible to determine the extent of local structural perturbations based on HX changes. However, since these two regions were highly solvent-exposed in native conformation, it was more likely for them to make contact with the ice surface.

The largest perturbations to LDH structure on freezing were located in reporter peptides 107–132, 170–204 and 288–331 (yellow in Fig. 5). It is interesting to note that they are adjacent to reporter peptides 91–108 and 205–237 described above, which are solvent-exposed in the native structure (see Fig. 5). By contrast, the blue- and slate-colored regions with less structural perturbations by freezing are located in the core of each monomer or at the interfaces between monomers in the native tetramer. Therefore, freezing seems to preferentially impact the surface residues of LDH, further supporting the mechanism of interface-induced protein denaturation during freezing.

In contrast to structural loss during a single freezing transition, repeated F/T cycles led to irreversible protein aggregation, the extent of which was influenced by the number of F/T cycles and protein concentration as suggested by HPSEC (Fig. 6). The partial structural denaturation and sequential protein aggregation observed in a single freezing step and after a number of F/T cycles, respectively, may be kinetically related as they are during solution phase protein aggregation. In general, non-native protein aggregation has been considered to take place through accumulation of partially unfolded intermediates that are more aggregation-prone relative to the native conformation (44). In F/T processing, the partially denatured LDH species observed in the frozen state may serve as the reactive intermediate for the aggregation process in the subsequent thawing step. This hypothesis was supported by the observation that freezing-induced LDH denaturation and aggregation after repeated F/T cycles both exhibited a similar protein concentration dependence.

However, it is worth noting that a single freezing step led to much less denaturation than seen in the LDH aggregates as a result of F/T cycles. In the freezing-induced denaturation, the structural perturbations were shown to be partial, and localized to the surface residues in Fig. 5. By contrast, LDH aggregation after F/T cycles caused comprehensive structure unfolding as suggested by ANS binding (Fig. 7) and HX analysis at both intact molecule and peptide level (Fig. 8 and 9). These differences suggest that formation of irreversible aggregates during F/T processing requires additional structure reorganization from the partially denatured species.

As described above, F/T-induced aggregates were made up of largely unfolded LDH. However, in Fig. 9, three short regions, 13–31, 109–117 and 133–143, showed moderate solvent protection in the aggregates. One possible cause of this protection is intermolecular interactions responsible for the F/T-induced LDH aggregation. This idea was reinforced by the consensus predictions of four different aggregation hotspot calculators (Fig. 10). In pharmaceutical development, identifying aggregation-prone segments in protein sequences could be of great interest, as it provides the potential targets for protein engineering to enhance protein stability against processing stresses. As indicated here, HX-MS could be a useful experimental approach to identify such critical polypeptide sequences for protein aggregation.

In summary, we have demonstrated the use of HX-MS as a new approach to analyze protein structure in the frozen state. Conformation population distributions and partially denatured states can be detected. In combination with in-line proteolysis, this approach also identified regions

of the protein that are susceptible to native structure loss caused by freezing. Further, the ice-solution interface was implied to be the primary factor for LDH denaturation as suggested by the preferential unfolding of surface residues. For irreversible aggregation, a more comprehensive pattern of conformational changes was observed. These results indicate HX-MS could be a valuable tool for detailed structure analysis of multidomain proteins such as monoclonal antibodies during F/T processing. The technique can also provide information about the nature of the aggregation behavior and structure of aggregates from this and other stresses, which is a key piece of information to understand the potential immunological impact of aggregation in biopharmaceuticals (45).

ACKNOWLEDGMENTS

The authors wish to thank Dr. Xiaoling Wang at BioTherapeutics Pharmaceutical Sciences, Pfizer Inc. for assistance with the PAGE calculations and Pfizer for financial support.

REFERENCES

1. Kolhe P, Holding E, Lary A, Chico S, Singh SK. Large-scale freezing of biologics: understanding protein and solute concentration changes in a cryovessel-Part I. Biopharm Int. 2010;23:53–60.
2. Kueltzo LA, Wang W, Randolph TW, Carpenter JF. Effects of solution conditions, processing parameters, and container materials on aggregation of a monoclonal antibody during freeze-thawing. J Pharm Sci. 2008;97:1801–12.
3. Jiang S, Nail SL. Effect of process conditions on recovery of protein activity after freezing and freeze-drying. Eur J Pharm Biopharm. 1998;45:249–57.
4. Strambini GB, Gabellieri E. Proteins in frozen solutions: Evidence of ice-induced partial unfolding. Biophys J. 1996;70:971–6.
5. Franks F, Hatley RHM. Low-temperature unfolding of Chymotrypsinogen. Cryobiology. 1985;22:608–8.
6. Griko YV, Privalov PL, Sturtevant JM, Venyaminov SY. Cold denaturation of staphylococcal nuclease. Proc Natl Acad Sci USA. 1988;85:3343–7.
7. Schwegman JJ, Carpenter JF, Nail SL. Evidence of partial unfolding of proteins at the ice/freeze-concentrate interface by infrared microscopy. J Pharm Sci. 2009;98:3239–46.
8. Chang BS, Kendrick BS, Carpenter JF. Surface-induced denaturation of proteins during freezing and its inhibition by surfactants. J Pharm Sci. 1996;85:1325–30.
9. Akers MJ, Milton N, Byrn SR, Nail SL. Glycine crystallization during freezing—the effects of salt form, ph, and ionic-strength. Pharm Res. 1995;12:1457–61.
10. Murase N, Franks F. Salt precipitation during the freeze-concentration of phosphate buffer solutions. Biophys Chem. 1989;34:293–300.
11. Cao EH, Chen YH, Cui ZF, Foster PR. Effect of freezing and thawing rates on denaturation of proteins in aqueous solutions. Biotechnol Bioeng. 2003;82:684–90.
12. Goller K, Galinski EA. Protection of a model enzyme (lactate dehydrogenase) against heat, urea and freeze-thaw treatment by compatible solute additives. J Mol Catal B Enzym. 1999;7:37–45.
13. Paborji M, Pochopin NL, Coppola WP, Bogardus JB. Chemical and physical stability of chimeric L6, a mouse-human monoclonal-antibody. Pharm Res. 1994;11:764–71.
14. Hawe A, Kasper JC, Friess W, Jiskoot W. Structural properties of monoclonal antibody aggregates induced by freeze-thawing and thermal stress. Eur J Pharm Sci. 2009;38:79–87.
15. Hillgren A, Lindgren J, Alden M. Protection mechanism of Tween 80 during freeze-thawing of a model protein, LDH. Int J Pharm. 2002;237:57–69.
16. Gabellieri E, Strambini GB. ANS fluorescence detects widespread perturbations of protein tertiary structure in ice. Biophys J. 2006;90:3239–45.
17. Dong JP, Hubel A, Bischof JC, Aksan A. Freezing-induced phase separation and spatial microheterogeneity in protein solutions. J Phys Chem B. 2009;113:10081–7.
18. Paborji M, Pochopin NL, Coppola WP, Bogardus JB. Chemical and physical stability of chimeric L6, a mouse-human monoclonal antibody. Pharm Res. 1994;11:764–71.
19. Kreilgaard L, Jones LS, Randolph TW, Frokjaer S, Flink JM, Manning MC, *et al.* Effect of Tween 20 on freeze-thawing- and agitation-induced aggregation of recombinant human factor XIII. J Pharm Sci. 1998;87:1597–603.
20. Rosenberg AS. Effects of protein aggregates: an immunologic perspective. AAPS J. 2006;8:E501–7.
21. Purohit VS, Middaugh CR, Balasubramanian SV. Influence of aggregation on immunogenicity of recombinant human factor VIII in hemophilia A mice. J Pharm Sci. 2006;95:358–71.
22. Smith DL, Deng YZ, Zhang ZQ. Probing the non-covalent structure of proteins by amide hydrogen exchange and mass spectrometry. J Mass Spectrom. 1997;32:135–46.
23. Garcia AE, Hummer G. Conformational dynamics of cytochrome c: correlation to hydrogen exchange. Proteins. 1999;36:175–91.
24. Houde D, Arndt J, Domeier W, Berkowitz S, Engen JR. Characterization of IgG1 conformation and conformational dynamics by hydrogen/deuterium exchange mass spectrometry. Anal Chem. 2009;81:2644–51.
25. Pan JX, Rintala-Dempsey AC, Li Y, Shaw GS, Konermann L. Folding kinetics of the S100A11 protein dimer studied by time-resolved electrospray mass spectrometry and pulsed hydrogen-deuterium exchange. Biochemistry. 2006;45:3005–13.
26. Cierpicki T, Bielnicki J, Zheng MY, Gruszczyk J, Kasterka M, Petoukhov M, *et al.* The solution structure and dynamics of the DH-PH module of PDZRhoGEF in isolation and in complex with nucleotide-free RhoA. Protein Sci. 2009;18:2067–79.
27. Zhang A, Qi W, Good TA, Fernandez EJ. Structural differences between A beta(1–40) intermediate oligomers and fibrils elucidated by proteolytic fragmentation and hydrogen/deuterium exchange. Biophys J. 2009;96:1091–104.
28. Lu XJ, Wintrode PL, Surewicz WK. Beta-sheet core of human prion protein amyloid fibrils as determined by hydrogen/deuterium exchange. Proc Natl Acad Sci USA. 2007;104:1510–5.
29. Li YS, Williams TD, Topp EM. Effects of excipients on protein conformation in lyophilized solids by hydrogen/deuterium exchange mass spectrometry. Pharm Res. 2008;25:259–67.
30. Anchordoquy TJ, Izutsu K, Randolph TW, Carpenter JF. Maintenance of quaternary structure in the frozen state stabilizes lactate dehydrogenase during freeze-drying. Arch Biochem Biophys. 2001;390:35–41.
31. Izutsu K, Yoshioka S, Terao T. Effect of mannitol crystallinity on the stabilization of enzymes during freeze-drying. Chem Pharm Bull. 1994;42:5–8.
32. Slavik J. Anilinonaphthalene sulfonate as a probe of membrane composition and function. Biochim Biophys Acta. 1982;694:1–25.
33. Levine H. Thioflavine-T interaction with synthetic alzheimers-disease beta-amyloid peptides - detection of amyloid aggregation in solution. Protein Sci. 1993;2:404–10.

34. Khurana R, Coleman C, Ionescu-Zanetti C, Carter SA, Krishna V, Grover RK, *et al.* Mechanism of thioflavin T binding to amyloid fibrils. J Struct Biol. 2005;151:229–38.
35. Kheterpal I, Chen M, Cook KD, Wetzel R. Structural differences in A beta amyloid protofibrils and fibrils mapped by hydrogen exchange—mass spectrometry with on-line proteolytic fragmentation. J Mol Biol. 2006;361:785–95.
36. Del Mar C, Greenbaum EA, Mayne L, Englander SW, Woods VL. Structure and properties of alpha-synuclein and other amyloids determined at the amino acid level. Proc Natl Acad Sci USA. 2005;102:15477–82.
37. Hoshino M, Katou H, Hagihara Y, Hasegawa K, Naiki H, Goto Y. Mapping the core of the beta(2)-microglobulin amyloid fibril by H/D exchange. Nat Struct Biol. 2002;9:332–6.
38. Fernandez-Escamilla AM, Rousseau F, Schymkowitz J, Serrano L. Prediction of sequence-dependent and mutational effects on the aggregation of peptides and proteins. Nat Biotechnol. 2004;22:1302–6.
39. Trovato A, Chiti F, Maritan A, Seno F. Insight into the structure of amyloid fibrils from the analysis of globular proteins. PLoS Comput Biol. 2006;2:e170.
40. Conchillo-Sole O, de Groot NS, Aviles FX, Vendrell J, Daura X, Ventura S. AGGRESCAN: a server for the prediction and evaluation of "hot spots" of aggregation in polypeptides. BMC Bioinformatics. 2007;8.
41. Tartaglia GG, Cavalli A, Pellarin R, Caflisch A. Prediction of aggregation rate and aggregation-prone segments in polypeptide sequences. Protein Sci. 2005;14:2723–34.
42. Zhang A, Jordan JL, Ivanova MI, Weiss WF, Roberts CJ, Fernandez EJ. Molecular level insights into thermally induced alpha-chymotrypsinogen a amyloid aggregation mechanism and semiflexible protofibril morphology. Biochemistry. 2010;49:10553–64.
43. Dobson CM. Protein folding and misfolding. Nature. 2003;426:884–90.
44. Singh SK. Impact of product-related factors on immunogenicity of biotherapeutics. J Pharm Sci. (2010).